



# Evolution and structure of a mesoscale anticyclonic eddy in the northwestern Japan Sea and its exchange with surrounding waters: in situ observations and Lagrangian analysis

Maxim V. Budyansky<sup>1</sup> · Svetlana Yu. Ladychenko<sup>1</sup> · Vyacheslav B. Lobanov<sup>1</sup> · Sergey V. Prants<sup>1</sup> · Aleksandr A. Udalov<sup>1</sup>

Received: 14 March 2024 / Accepted: 24 July 2024 / Published online: 14 October 2024  
© Springer-Verlag GmbH Germany, part of Springer Nature 2024

## Abstract

Based on Lagrangian analysis we have found a region in the northwestern Japan Sea north of the Subpolar Front where mesoscale eddies regularly form and circulate. The strong anticyclonic eddy, vertically extended to the bottom with multilayer core structure and extreme values of temperature and salinity was sampled in this region during the cruise of R/V *Akademik M.A. Lavrentyev* in May 2004. The altimetry-based eddy tracking showed that it had a life span of nine months with the size reaching 120 km. CTD observational data were used to explore the eddy's features and vertical structure. The eddy had a multilayer core with different thermohaline characteristics, was observed in this area for the first time and could be originated due to its interaction with the surrounding water. The evolution of the eddy, origin of water inside the eddy core and the water 'age' on every day of the eddy's life have been studied and analyzed with the help of altimetry-based Lagrangian indicators of water motion. Inspecting daily-computed Lagrangian maps, we documented the essential events in the evolution of the eddy including its formation, splitting, merger, entrainment and detrainment of water, erosion and eventual decay. All these observations have been verified with the infrared satellite images. It has been found that the surface core has been filled mainly with subtropical water originated in the southern flank of the Subpolar Front.

**Keywords** Northwestern Japan Sea · Mesoscale eddy · Evolution and structure · Lagrangian analysis

## 1 Introduction

The circulation of the Japan Sea (JS) basically consists of the Tsushima Warm Current (TWC) system that transports warm subtropical water from the south through the Korea Strait (Fig. 1a) by two main streams: a near shore branch of TWC that flows eastward and northward along Japan and East Korea Warm Current (ECWC) flowing northward along Korea. In the northern part of the JS, the Primorye (Liman) Current and its continuation, the North Korea Cold Current transport subarctic waters to the southwest along

the coast of Russia and North Korea (Uda 1934; Yarichin 1980; Yurasov and Yarichin 1991; Preller and Hogan 1998; Chang et al. 2016).

The confluence of subtropical and subarctic waters forms the distinct Subpolar Front in the Japan Sea (JS), that lies between 39° and 41°N and extends across the whole basin from the Korean coast to the Japanese islands (Park and Chung 1999; Park et al. 2004; Talley et al. 2006; Lee et al. 2006; Yoshikawa et al. 2012; Zhao et al. 2014; Wagawa et al. 2020) (Fig. 1). The zonal eastward flow along the front is known to be highly variable with seasonal migration (Chang et al. 2004; Yoon et al. 2009). Meandering of the frontal flow is accompanied with formation of eddies of different polarity and size generated through a baroclinic instability (Ou and Gordon 2002; Lee and Niiler 2005, 2010). In the previous studies, anticyclonic eddies (ACEs) have been often observed in the area north of Yamato Rise in satellite images (Sugimoto and Tameishi 1992; Ginzburg et al. 1998; Lobanov et al. 1998; Morimoto et al. 2000; Nikitin et al.

---

Responsible Editor: Yasumasa Miyazawa

---

✉ Sergey V. Prants  
prants@poi.dvo.ru

<sup>1</sup> V.I. Il'ichev Pacific Oceanological Institute, Far Eastern Branch, Russian Academy of Sciences, 43 Baltiyskaya St., Vladivostok 690041, Russia

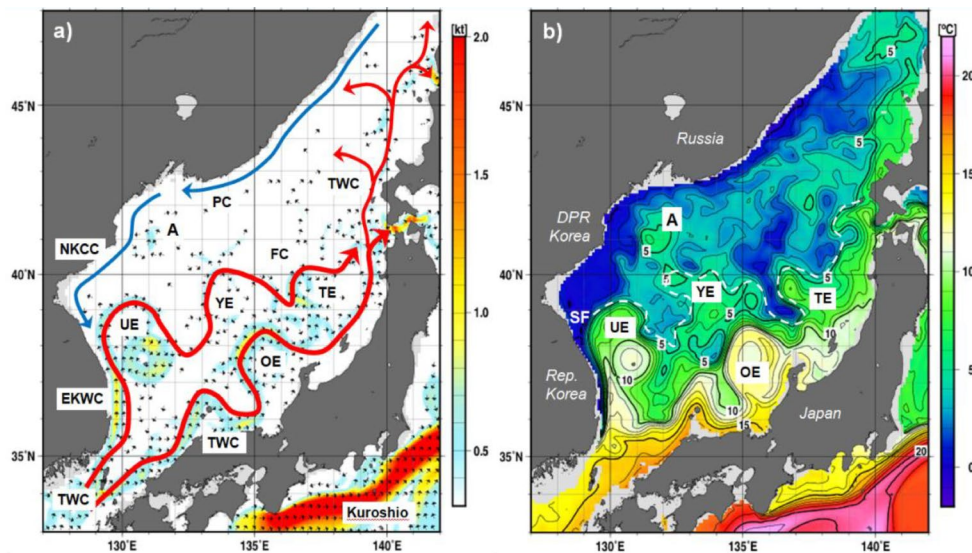


**Fig. 1** (a) Scheme of the main currents in the Japan Sea based on Refs. (Uda 1934; Yarichin 1980; Yurasov and Yarichin 1991; Preller and Hogan 1998; Chang et al. 2016) overlapped on the map of 10-day mean currents at 50 m for 11–20 May 2004. Direction of currents is shown by small arrows, and the speed of currents is shown by color in knots. (b) Temperature distribution at 100 m depth for the same period, JMA data (<https://www.data.jma.go.jp/>). TWC – Tsushima Warm Cur-

rent; EKWC – East Korea Warm Current; PC – Primorye (Liman) Current; NKCC – North Korea Cold Current; FC – Frontal Current. Subpolar Front is indicated by the white dashed line (SF) in b). Warm-core anticyclonic eddies are observed to the north of the front (A), over Yamato Rise (YE), in the Ulleung Basin (UE), east of Oki Spur (OE) and at other locations. Location of the studied anticyclonic mesoscale eddy on these dates is indicated as A

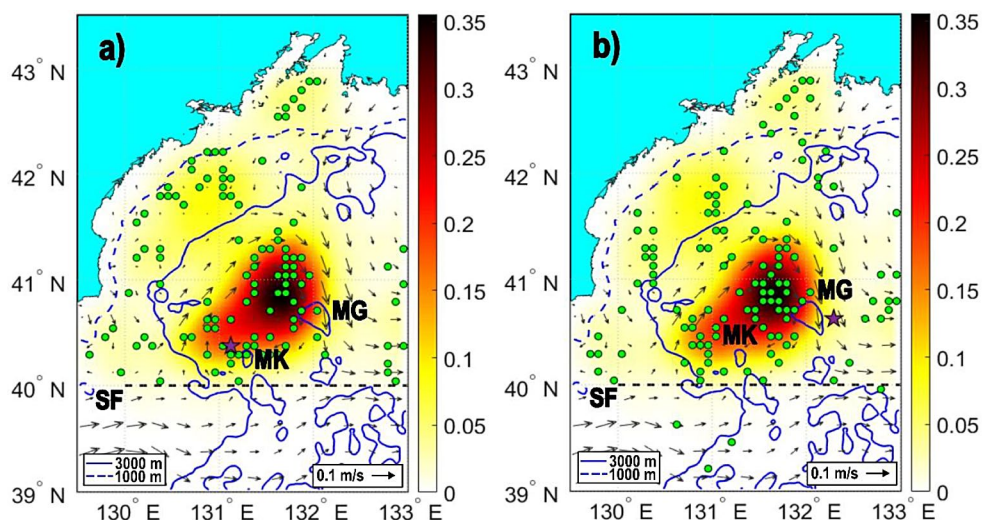
2012; Kim et al. 2021; Trusenkova and Kaplunenko 2022), in the current meter observations at the mooring station M3 (Takematsu et al. 1999) and during oceanographic surveys (Chang et al. 2016; Lobanov et al. 1998, 2007; Nikitin et al. 2002). The topographically controlled mesoscale ACEs have been simulated in Prants et al. (2015) with the help of a numerical circulation model that showed the formation and stagnation of such eddies during the cold season over sea mounts and bottom depressions. The quasi-stationary ACEs have been shown to be sufficiently nonlinear to exist as a stable entity. The quasigeostrophic nonlinearity parameter (the ratio of the relative vorticity advection to the planetary vorticity advection) has been estimated to be in the range of 3.3–6.6 (Prants et al. 2015).

The quasi-stationary frontal eddies in the northern JS have been sampled and studied much more rarely than quasi-stationary eddies in the southern part of the Sea like the warm Ulleung quasi-stationary ACE in the Ulleung Basin (Chang et al. 2004; Gordon et al. 2002; Shin et al. 2005; Shin 2009; Hogan and Hurlburt 2006), the ACE over bottom topography around Yamato Rise (Isoda et al. 1992; Isoda and Nishihara 1992) and the Oki Spur, the Wonsan ACE (Lee and Niiler 2005), the Doc cyclonic eddy in between the Ulleung and Oki ACEs (Mitchell et al. 2005), and eddies in the eastern area of Tsushima Current (Isoda 1994; Yabe et al. 2021). All these eddies have been well studied with the help of ship and satellite observations, surface drifters and profiling floats.

In this paper, we have analyzed another area to north of the Subpolar Front in the northwestern JS where mesoscale eddies regularly form, circulate and decay (Fig. 2). The frontal eddies in the northwestern JS are also interesting because they form in the area where warm subtropical and cold subarctic waters mix with an impact on marine ecosystem. It may be important for understanding transport pathways for invasion of subtropical species (Nikitin et al. 2002; Prants et al. 2017a). Since the last decades in the twentieth century, invasion of warm-water fish (conger eel, tuna, moonfish and triggerfish) and some tropical and subtropical marine organisms (turtles, sharks and others) has been increasingly observed near the coast of Russia (Ivankova and Samoilova 1979).

We study a frontal ACE, called hereafter eddy A, in the northwestern JS that was sampled in May 2004 (Fig. 1). This large-scale eddy lasted an exceptionally long time as an entity allowing us to track its evolution from formation to decay with the help of altimetry-based Lagrangian indicators. The Lagrangian analysis is used to document the essential events in the evolution of this eddy and to identify the origin of water masses that were gained, retained, and released by the eddy and to compare the simulation results with ship observation data and satellite infrared images. For this purposes, the Lagrangian approach seems more suitable than commonly used Eulerian means because the Lagrangian maps are imprints of the history of water involved in the vortex motion, whereas vorticity, the Okubo-Weiss

**Fig. 2** The occurrence frequency of anticyclones (see Sect. 2.2) with the lifespan exceeding 30 days in the northwestern Japan Sea in 1993–2021 with the superimposed formation (a) and decay (b) sites. The sites of formation and decay of eddy A are shown in (a) and (b) by stars on January 9 and October 10, 2004, respectively. The mean altimetric velocity field is shown by arrows. MG and MK are locations of seamounts Gabass (40.30°N, 132°E) and Kol'tso (40.30°N, 131°E). The mean position of the Subpolar Front is shown by the dashed black line. The blue curves are the 1,000 and 3,000 m isobaths



parameter and similar Eulerian indicators are just ‘instantaneous’ snapshots.

The paper is organized as follows. The CTD data obtained from the shipboard observations and satellite data are described in Sect. 2. Section 2 introduces also the automated tracking algorithm for detection of eddies and Lagrangian methods that we used in the present paper. Section 3 presents the area of the most frequent formation of anticyclonic eddies just to the north of Subpolar Front by AMEDA algorithm, and the eddy A vertical structure and composition of water masses in its core using the results of shipboard observations. In Sect. 4, we document the essential events in the eddy’s evolution based of Lagrangian maps and compare the simulation results with satellite infrared images. Calculation of the evolution of the content of waters of subtropical and subarctic origin within the eddy core is also presented in Sect. 4. The results are discussed in Sect. 5.

## 2 Materials and methods

### 2.1 Shipboard observations and satellite data

Ship observations in the study area, shown in Fig. 2, were implemented during the cruise of R/V *Akademik M.A. Lavrentyev* in May 11–16, 2004 (cruise No. 33). The eddy was identified by the NOAA satellite infrared images as a circular shaped area of warm water located between 40°30′–41°40′N and 131°30′–133°00′E with the diameter of about 120 km. Two sections crossing the eddy from south to north and from west to east with CTD profiles down to the bottom (about 3400 m) were performed. The first, south-north section along 132°20′E with a distance between the CTD stations of 27–30 km was used to found an approximate location of the eddy center by the maximum downward

deflection of the temperature and salinity isolines, while the second, west-east section along 41°09′N was done with a closer location of the stations (10–12 km) and expectedly crossing the eddy closer to its center. Every other station of this section was limited to 1500 m to save a ship time. The Neil Brown Mark-III CTD instrument was used in this survey. The data on water temperature and salinity profiles was averaged to 1 m intervals and the plots were made using the Ocean Data View software (Schlitzer 2023).

NOAA AVVRR satellite infrared images for the operational and post cruise analysis were provided by Regional Satellite Monitoring Center of Far Eastern Branch of Russian Academy of Sciences (<http://www.satellite.dvo.ru>). We also used maps of water temperature and currents provided by Japan Meteorological Agency (<https://www.data.jma.go.jp>).

### 2.2 Lagrangian methods

We use the altimetric geostrophic velocities derived from the absolute dynamic topography maps, produced by Salto/Duacs (<https://www.aviso.altimetry.fr>) and distributed by the Copernicus Marine Environment Monitoring Service (CMEMS L4 product) with a spatial resolution 1/4°×1/4° and daily time step. To identify mesoscale eddies, we apply AMEDA (Angular Momentum Eddy Detection and tracking Algorithm) based on the altimetric geostrophic velocities (Le Vu et al. 2018).

The algorithm consists of (i) detecting the eddy’s centers, (ii) computation of the streamlines surrounding the center, and (iii) computation of the mean eddy’s radius and swirl velocity along each closed streamline. The characteristic radius, at which the maximum swirl velocity is reached, is used to quantify the lateral eddy size. The characteristic contour of a detected eddy is associated with a closed streamline of the maximal swirl speed. The algorithm is robust to the grid resolution, uses a minimal number of parameters

and provides a description of the complete dynamical evolution of detected eddies. In difference from the algorithm in Chelton et al. (2011) and the META3.2 algorithm (Pegliasco et al. 2022), AMEDA gives a more realistic estimate of the size of the identified eddies and allows us to document merging and splitting of eddies as well.

To calculate occurrence frequency of anticyclones the study area was covered by boxes with the size of  $0.1^\circ \times 0.1^\circ$ . Every day during the observation period (1993–2021), the contours of identified long-lived eddies were superimposed on this grid to calculate how many times  $N$  each grid point fell within the contour of an individual eddy. The occurrence frequency at a given place equals  $N/\Sigma$  and is modulated by color in figures, where  $\Sigma$  is the total number of the observation days (10,592).

To identify and track locations of the eddy's centers, we computed the points where the daily-averaged velocity is zero. The stationary or fixed points are specified as locations where the daily-averaged velocity is zero. To study a character of motion nearby a stationary point the components of velocity  $u$  and  $v$  are expanded in a Taylor series. The corresponding linearized advection equations are analyzed by the standard stability analysis of linearized equations of motion (see, e.g., Prants et al. 2017b). By the type of stability, we distinguish elliptic and hyperbolic stationary points. The elliptic points are stable ones being usually located in the centers of eddies, where rotation prevails over deformation. The hyperbolic points are unstable ones being located around and between eddies, where deformation prevails over rotation. The stationary points in the ocean are Eulerian objects of the 'frozen' velocity field. They can move in the course of time, but they are not trajectories of water elements.

In the Lagrangian approach, the transport and mixing processes are studied by following fluid parcels to identify the trajectories and to reveal all possible pathways of water from one location to another one. Trajectories of virtual passive particles, distributed in the study area over a grid with  $350 \times 350$  nodes, are computed integrating advection equations

$$\frac{d\lambda}{dt} = u(\lambda, \phi, t), \quad \frac{d\phi}{dt} = v(\lambda, \phi, t) \quad (1)$$

with the fourth-order Runge-Kutta scheme. In Eq. 1,  $u$  and  $v$  are angular zonal and meridional components of the altimetric velocity field,  $\phi$  and  $\lambda$  are latitude and longitude of a Lagrangian particle. Angular velocity is related to linear velocity by the formula (Prants et al. 2022)

$$u = \frac{0.864}{1.853} \frac{1}{\cos\phi} U, \quad v = \frac{0.864}{1.853} V$$

where  $u$  and  $v$  are expressed in arc minutes per day, and  $U$  and  $V$  are given in cm/s. The velocity field is interpolated in space and time (for details of computation, see, e.g., Prants et al. 2017b). We have not computed trajectories of the particles that reached coastal AVISO cells of the size of  $1/4^\circ \times 1/4^\circ$  where the altimetric velocity field is unreliable. These trajectories stopped when reaching the coastal cells.

Exclusive to Lagrangian particle experiments is that the entire trajectory history of the virtual particles can be stored. Another advantage of these experiments is that particles can be advected backwards in time when velocity fields are stored. This reverse-time method allows us to investigate where water masses in the study area or within eddies came from.

To find and document the main events in the eddy's life-cycle (formation, strengthening, merger, splitting, deformation, weakening, erosion and decay), we use the Lagrangian diagnostics based on calculation of specific indicators of motion of passive particles mimicking water parcels. We use in this study three kinds of Lagrangian indicators. For each virtual particle, the length of its trajectory,

$$L = R \int_0^T \sqrt{(\lambda'(t))^2 \cos^2\phi(t) + (\phi'(t))^2} dt, \quad (2)$$

is calculated backward in time for  $T=30$  days by integrating advection Eq. (1). Here  $(\phi(t_1), \lambda(t_1))$  and  $(\phi(t_2), \lambda(t_2))$  are initial and final positions of the particle,  $\phi'(t)$  and  $\lambda'(t)$  are time derivatives,  $R=6371$  km is the Earth's radius. The values of  $L$  in km are represented by a gradation of gray color on the path maps (L-maps) (Ponomarev et al. 2018). These maps are parameterized by the starting date and the integration period  $T$ . Each L-map contains information about the paths travelled by a considerable number of virtual particles for  $T=30$  days prior to the date indicated on the L-maps. The L-maps allow us to track evolution of eddies and to document the processes of entrainment and detrainment of water by eddies.

In order to identify the origin of water inside vortex cores, we compute the origin maps (O-maps) (Ponomarev et al. 2018). Integrating advection Eq. (1) backward in time, we determine which geographical border of the study area the virtual particles crossed in the past. The O-maps are parameterized by the starting day and the maximum integration period which has been found empirically to be  $T=360$  days. The particles are colored on the O-maps in accordance with the border that they crossed for 360 days prior to the date indicated on the maps.

The 'age' of water in the study area is determined with the help of the 'age' maps (T-maps) (Ponomarev et al. 2018). They show how much time it takes for each particle to reach its place on a map after crossing one of the boundaries of the

study area for 360 days in the past. All the Lagrangian maps are computed daily. The O-, L- and T- maps provide us with complementary information on kinematics and evolution of the studied features. We also used sea surface temperature data from satellites MODIS Aqua/Terra. It should be mentioned that the Lagrangian maps give information on the movement, history, origin and ‘age’ of water but not about change of hydrological properties due to mixing with the background water.

### 3 Eddy location and vertical structure

#### 3.1 Area with the frequent occurrence of Eddies

To identify and track locations of the eddy centers, we compute the elliptic points (see Sect. 2.2). The color in Fig. 2 shows the occurrence frequency of all ACEs in 1993–2021. The sites of formation and decay of the ACEs with the lifespan exceeding 30 days are shown in Fig. 2a and b, respectively. The place with increased occurrence frequency is clearly seen to the north off the Subpolar Front in the northwestern JS. Although the ACEs have been observed in this area (Lobanov et al. 1998, 2007; Nikitin et al. 2002, 2012), as far as we know, this place was mentioned as an area with a high occurrence frequency of ACEs only in one paper (Lee et al. 2019). However, formation and decay mechanisms of these eddies, their distribution and features of their evolution have not been studied enough. Based on AMEDA results, the studied eddy A, which was formed in January, sampled in May and decayed in October 2004 circulating all its lifetime in this area. Its evolution will be discussed in Sect. 4.

#### 3.2 Vertical structure of the Eddy A

In spring 2004, the anticyclonic mesoscale eddy A was clearly visible in the northwestern JS by both satellite infrared images and routine hydrographic data. Figure 1 shows water temperature distribution at 100 m during 11–20 May provided by the Japan Meteorological Agency (JMA, <https://www.data.jma.go.jp/>). The eddy A can be easily identified as an isolated pool of warm water ( $> 5^{\circ}\text{C}$ ) between  $40^{\circ}30'$  and  $41^{\circ}30'$  and  $131^{\circ}00'$ – $132^{\circ}30'$ E with a circular shape of about 120 km in diameter. It seems that it was the strongest mesoscale feature in the distribution of 100-meter temperature in the northwestern part of the JS.

Infrared images of NOAA satellites (Fig. 3a) demonstrated more details of the eddy A structure. It has a shape of the hoop with outer diameter around of 100 km formed by warmer water of  $10$ – $11^{\circ}\text{C}$  at its edge intruded from the south and slightly colder central part ( $9$ – $10^{\circ}\text{C}$ ). Subpolar

front with warmer water ( $> 12^{\circ}\text{C}$ ) is located just 30–50 km to the south of the eddy.

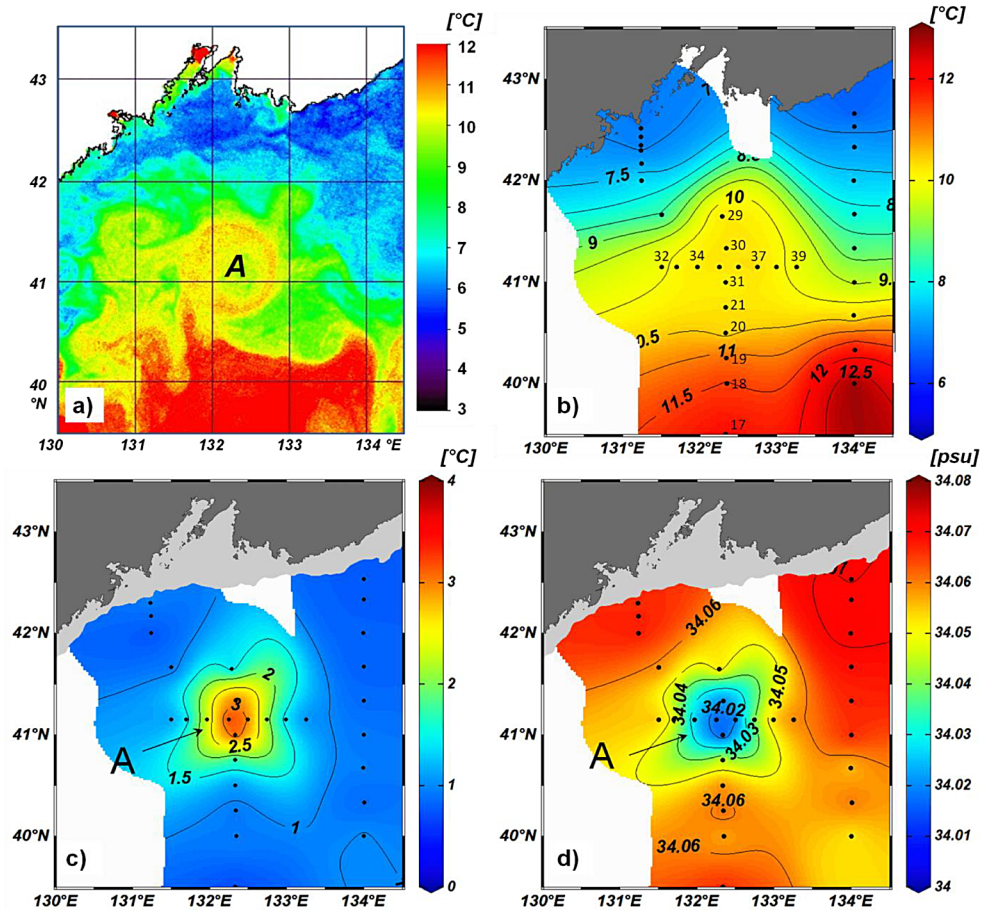
The results of the ship CTD observations are presented in Fig. 3b, c and d. The eddy is not clear visible at the surface temperature (Fig. 3b) because of sparse spatial distribution of the CTD stations. However, it was clearly visible as a warm water area in the subsurface layers. As an example, Fig. 3c shows the eddy at the depth of 300 m. It is seen as an area of a temperature  $> 3^{\circ}\text{C}$  while surrounding water was below  $1.5^{\circ}\text{C}$ . In the salinity field at 300 m, in opposite, the eddy was manifested as a low salinity area, below 34.0 psu. This is determined by peculiarities of its thermohaline structure discussed below.

Figure 4a shows a spatial distribution of dynamic height (dynamic topography) at the sea surface calculated relative to 1500 m. Geostrophic currents were maximal in the surface layer and reached up to 50 cm/s at a distance of 40 km from the eddy center (Fig. 4b). The current velocity decreased with the depth but it was above 15 cm/s at 300 m. The eddy has a conical shape where a zone of maximum velocities was shifted toward the eddy center with a depth and was located about 25 km from the center at 300 m. Even below this depth, the currents in the eddy exceeded 10 cm/s. Such a high current velocity proves that the eddy A was strong enough to determine water circulation in the area of its location.

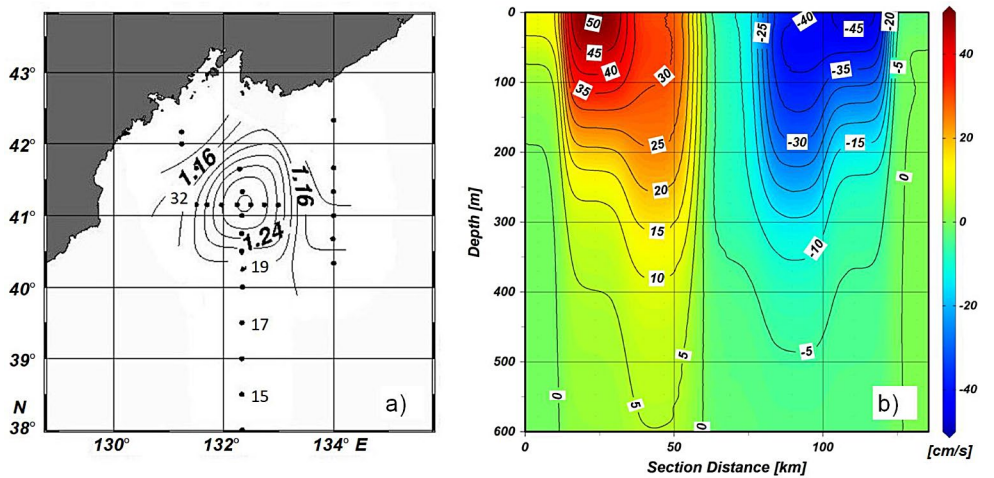
Vertical distributions of water temperature and salinity across the eddy were typical for ACEs in the northern JS (Talley et al. 2006; Lobanov et al. 1998, 2007; Nikitin et al. 2002). The eddy A seems to make the most significant anomaly in the vertical distribution of oceanographic parameters along this section. The downward curvature of the temperature, salinity and potential density isolines was traced down to the bottom or at least to the depth of 2700–3000 m (Fig. 5). Extremely uniform bottom layer of the JS makes it hardly possible to trace horizontal inhomogeneities associated with the eddy in the very bottom layer. Deep penetration of the eddy allows us to conclude on the strong barotropic component of anticyclonic rotation in the eddy.

Section of potential temperature (Fig. 5a) shows warm surface water ( $> 11$ – $12^{\circ}\text{C}$ ) south of the Subpolar Front. This water has the highest salinity up to 34.10–34.15 psu (Fig. 5b). Vertical distribution of salinity shows typical structure for the JS with low salinity intermediate water at depth of 100–250 m, high salinity intermediate water at 300–700 m and deep salinity minimum around 1500–1800 m (Talley et al. 2006; Lobanov et al. 2007; Kim et al. 1999; Watanabe et al. 2001). However, this structure is changed inside the eddy A. There is a core of low salinity water at 250–400 m (LS), another core of higher salinity water at 50–200 m (HS1) and a core of high salinity intermediate water (HS2) deepened down to 700–1100 m.

**Fig. 3** (a) Infrared image from NOAA-12 satellite on May 13, 2004 at 20:46 and distribution of (b) surface temperature, (c) temperature at 300 m and (d) salinity at 300 m based on the ship CTD observations during 11–16 May, 2004. Locations of the CTD stations 17–21 and 29–39 across the studied eddy A are indicated by black dots



**Fig. 4** (a) Dynamic topography of the sea surface relative to 1500 m (dyn m) and (b) vertical distribution of the meridional component of geostrophic velocity (cm/s) along the Sect. 41°09'N crossing the eddy A. The results are based on the ship CTD observations in 11–16 May, 2004. Red and blue color correspond to northward and southward flows. Locations of the CTD stations 17–21 and 29–39 across the studied eddy A are indicated by black dots



More detailed structure of the eddy A can be seen at the zonal section along 41°09'N with better spatial resolution. Temperature section (Fig. 6a) shows a surface layer of warm water (8.5–10.5 °C) underlined by forming seasonal thermocline at the depth of 20–30 m. This water within the eddy marked as WI has a higher salinity (33.98–34.0 psu) than surrounding surface waters (33.8 psu) and probably originates in the southern Subpolar Front area being advected

from south as it is demonstrated on the satellite image in Fig. 3a).

Below a seasonal thermocline in the layer from 30 to 230 m, one can see a comparatively uniform water of 6–8 °C and higher salinity (34.03–34.05 psu) marked as UC and HS1 in Fig. 6a and b. This water is not typical for the vertical structure of waters in the northern JS. Deeper, between 250 and 400 m in the eddy center, one can see a low

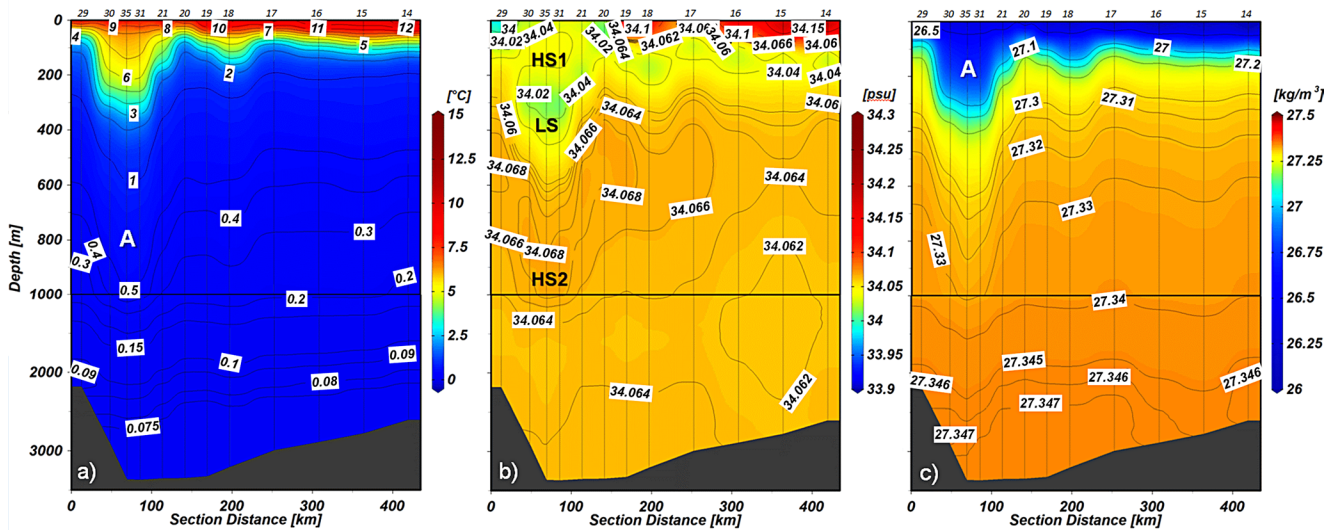


**Fig. 5** (a) Potential temperature, (b) salinity and (c) potential density anomaly distributions along the meridional section (along 132°20'E from 38°00'N to 41°40'N) crossing the eddy A based on the CTD observations in 11–14 May, 2004. HS1 – upper high salinity layer; LS – low salinity core; HS2 – lower high salinity layer. Thin vertical lines

mark the CTD stations, the station numbers are indicated at the top. Locations of the stations are shown in Fig. 3. Isolines are drawn with an irregular step. Vertical scale is different in the ranges of 0–1000 m and 1000–3500 m

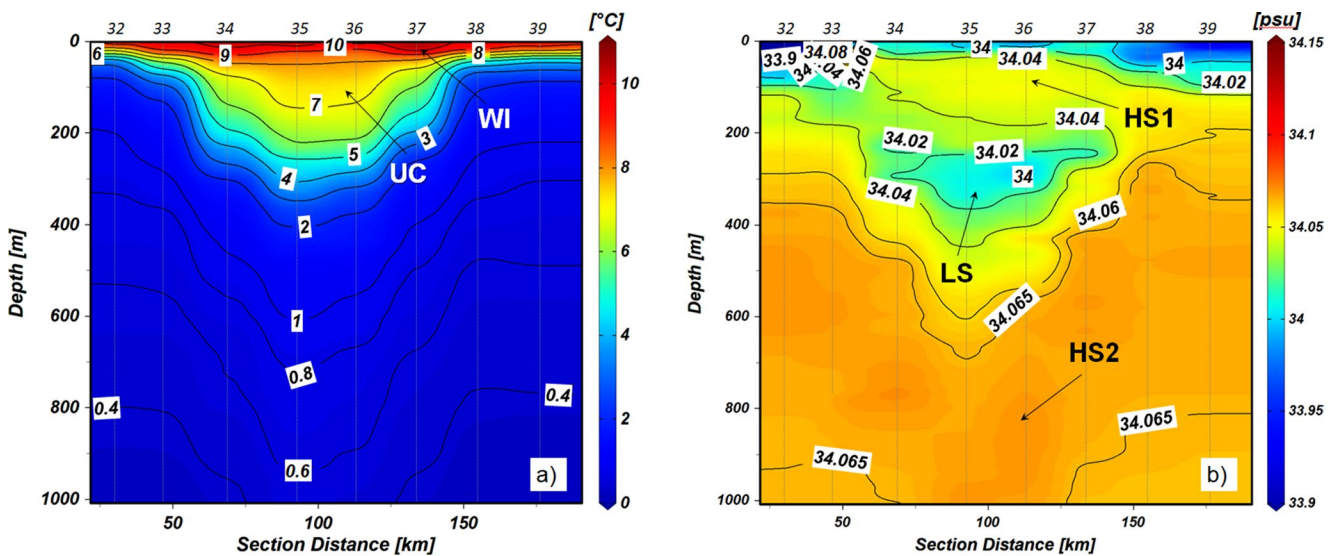


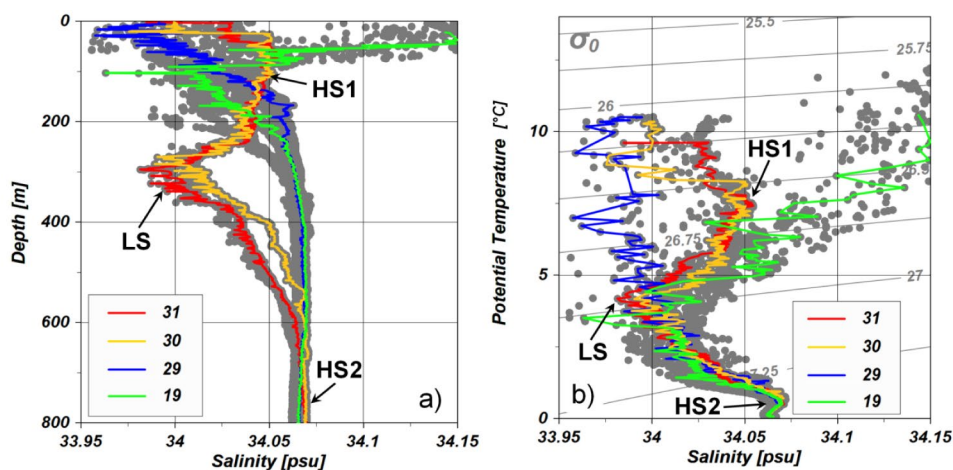
**Fig. 6** (a) Potential temperature and (b) salinity distributions along the zonal Sect. (41°09'N) crossing the eddy A based on the CTD observations during 14–16 May, 2004. WI – warm intrusion; UC – vertically uniform core; HS1 – upper high salinity layer; LS – low salinity

core; HS2 – lower high salinity layer. Thin vertical lines mark the CTD stations, the station numbers are indicated at the top. Locations of the stations are shown in Fig. 3. Isolines are drawn with an irregular step

salinity layer (LS) where salinity decreases down to 33.97 psu which corresponds to low salinity intermediate water in the JS, but in the eddy center it is located much deeper than in surrounding waters. Similar to this, an intermediate salinity maximum associated with a core of the JS high salinity intermediate water (HS2) deepened down to 1000 m in the eddy center, which is much deeper than in surrounding waters in the northern JS (400–600 m).

One may suggest that the anomalies in salinity vertical profile inside the eddy are very small and negligible. However they are significant for the JS, as it has extremely uniform vertical distribution of TS parameters below 100–200 m (Talley et al. 2006). Salinity values below 200 m and down to 3500 m vary in a very narrow interval, between 34.02 and 34.07 psu. To prove this we plotted a TS-diagram and vertical profiles of salinity for all stations of the Sect. 132°20'E (Fig. 7). Thus, low salinity core of the

**Fig. 7** (a) Vertical profiles of salinity at all stations of the section along 132°20'E and (b) TS-diagram for these stations. Profiles at two stations within the eddy A (#30 and #31) and two stations just outside the eddy (#19 and #29) are marked by different colors. Locations of the stations are shown in Fig. 3. For the other symbols see Figs. 5 and 6



anticyclonic eddy (LS) with salinity values down to 33.98 psu at the depth of 300 m seems a quite prominent anomaly. The same is valid for the upper high salinity core of the eddy at 50–250 m (HS1). This water with salinity around 34.05 psu has not been observed at this depth and at this isopycnal surface outside of the eddy. Subsurface water to the north has lower salinity while water to the south has much higher salinity. This core (HS1) has an almost uniform density. One can assume that this water was entrained and trapped during eddy formation in the frontal zone and transported as it evolved.

An unusual feature of the eddy vertical structure is a presence of a few layers with anomalous water in its central part. This multilayer structure of the eddy may be the result of its interaction with the surrounding waters and neighbor eddies and fronts, as well as merging and splitting during its evolution. We will analyze this below.

#### 4 Lagrangian Analysis of Evolution of the Eddy

The altimetry-based L-, O- and T- maps were computed daily (see Sect. 2.2) and analyzed in this section to study the evolution of the studied eddy and some of its properties. The inspection of the Lagrangian maps allows us to track and study the eddy over the lifetime. To validate the simulation results, we use SST images obtained on the same dates as the Lagrangian maps.

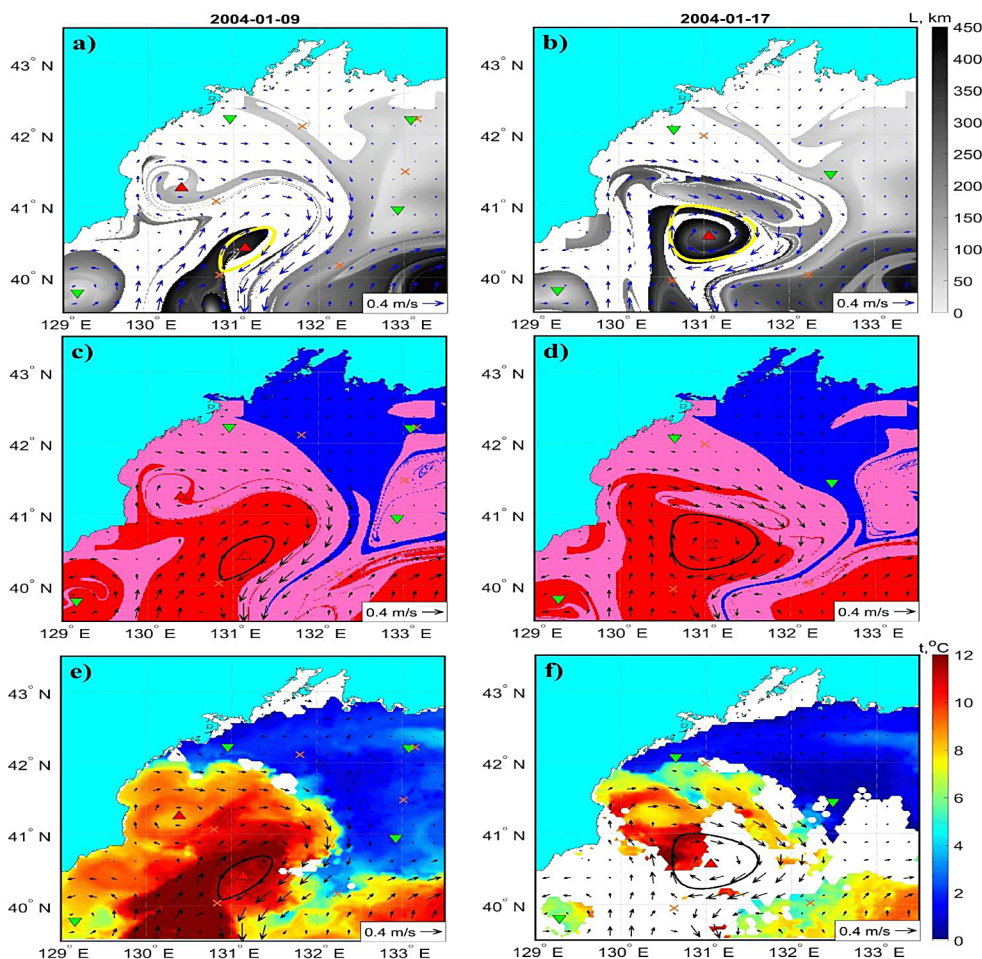
The eddy was formed from a meander-like feature of the Subpolar Front. The elliptic point, that was the center of the newborn eddy, appeared on Lagrangian maps in Fig. 8a and c on January 9, 2004 at (40.4°N, 131.2°E) signaling its birth. The red color on the O-maps in Fig. 8c and d codes the Lagrangian particles which crossed the Subpolar Front from south for 365 days prior the dates indicated on the maps. More exactly, they crossed during this period of time

the 39°N latitude somewhere in the range of 127°–140°E and represent subtropical water. The blue color codes the particles which crossed the 42.6°N latitude from north, and they represent subarctic water. The rose color codes water parcels which got into AVISO coastal grid cells for 365 days prior the dates indicated on the maps. Calculation of trajectories of particles backward in time was stopped when they reached one of the coastal AVISO cells. These Lagrangian particles represent coastal waters.

It follows from the Lagrangian maps in Fig. 8c and d that the eddy was filled up with a subtropical ‘red’ water. This water invades the area with a ‘rose’ coastal water. The eddy grew fast and reached ~80 km in diameter during the week after formation (Fig. 8b and d). The darker the color on L-maps, the greater the distance the corresponding particles traveled in the past. The spiral-like filament of the ‘dark blue’ water in Fig. 8b illustrates clearly the process of eddy formation. The SST images in Fig. 8e and f, taken on the same dates as the shown L- and O-maps, confirm the Lagrangian simulation, including formation of the eddy from the intrusion of subtropical water.

Inspecting the gallery of daily computed L- and O-maps and infrared images, we have found that the eddy experienced some deformations over the lifetime including events with entrainment and detrainment of water, splitting and merger with other eddies and eventual decay in October 2004. The first splitting of the eddy occurred a month after the formation between 15 and 25 February. Figure 9 shows how the splitting looks on L- and O-maps and SST images. A blob-like feature with the ‘dark grey’ water in Fig. 9a, split off from the parent eddy in the second half of February. The birth of an elliptic point at (41.3°N, 132°E) signaled appearance of the newborn eddy (Fig. 9b). This splitting is also seen on the SST images in Fig. 9c and d where the newborn eddy contained slightly colder water in the surface core as compared to the core of the parent eddy. During the splitting process, the vortex contour deformed and the streamers

**Fig. 8** Backward-in-time Lagrangian maps and SST images in January 2004. **(a)** and **(b)** L-maps, **(c)** and **(d)** O-maps with the superimposed AVISO velocity field show the eddy formation. Gradation of the gray color on these and other L-maps shows the length of the path covered by the virtual particles for 30 days in the past prior to indicated date. The white regions on the L-maps and rose regions on the O-maps correspond to the particles which came from the coastal regions to the final positions on the maps. Red and blue colors on the O-maps code subtropical and subarctic waters, respectively. The black curves on the O-maps and SST images are characteristic contours of the studied eddy (see Sect. 2.1) delineating the surface core. **(e)** and **(f)** SST images on the same dates as the Lagrangian maps (white color means cloudiness). The up (down) oriented red (green) triangles denote elliptic points corresponding to the locations of the centers of anticyclones (cyclones). The crosses are hyperbolic points



with ‘blue’ and ‘rose’ waters entrained into the vortex core (Fig. 9e and f).

Just after splitting, the parent eddy began to interact intensively with the newborn eddy. As the result, it eventually absorbed the newborn eddy. This process was signaled by disappearance of the elliptic point of the newborn eddy on March 5 (Fig. 10a). The united eddy has grown up gradually and reached almost circular shape by the beginning of April with the diameter of 100 km (Fig. 10b). The O-maps in Fig. 10c and d allow us to identify the subtropical origin of the water wrapped onto the eddy core. The process is complicated with the entrainment of a small amount of ‘blue’ subarctic water and ‘rose’ coastal water. The O-maps demonstrate narrow rings of waters of different origin around the eddy periphery. The entrainment process is seen in the SST field as well (Fig. 10e and f) but only partially due to cloudiness in the beginning of March.

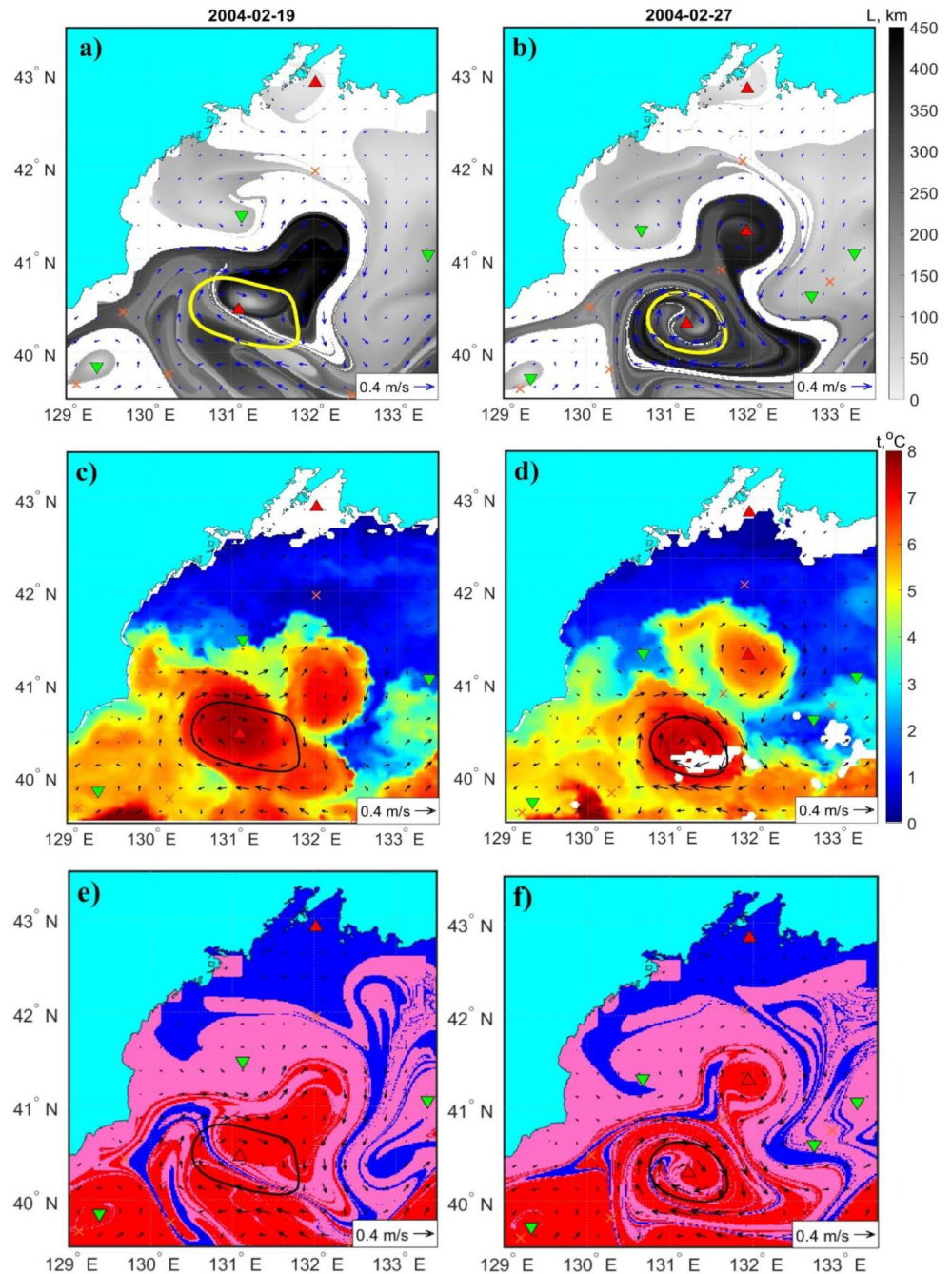
Just before sampling, the eddy again entrained water from the surrounding (Fig. 11). The L-maps in Fig. 11a and b show a streamer of this water as the long blue ‘tail’ from north. It follows from Fig. 11c and d that the streamer carried mostly a subtropical ‘red’ water. SST images in Fig. 10e and f confirm that. The entrainment process had started in

the end of April and continued until the days of sampling (May 11–16).

The information on the ‘age’ of water in the study area, and in particular, within the surface eddy core, can be obtained from T-maps computed for 365 days backward in time (see Sect. 2.2). The T-map in Fig. 12a shows the studied eddy on the day of sampling when it has the maximum lateral size. By this time, the eddy predominantly consisted of a subtropical water shown in grey which spent in the study area between 100 and 200 days. The darker the grey color, the older the core water is. The green and rose colors represent the ‘age’ of the coastal water. In other words, the green and rose particles got into the AVISO coastal grid cells for 365 days prior the dates indicated on the maps, and after that they were not integrated. Inclusions of the comparatively ‘young’ coastal water are present not only along the eddy periphery but inside the core as well.

The gradual erosion of the eddy resulted in a significant reduction of the eddy size (Fig. 12b and c). The interaction of the weakened eddy A, filled with the ‘old’ subtropical water, with a young ACE of the Subpolar Front to south (see the red triangle at 40°N, 131°30’E) is shown in Fig. 12b on August 17. By this time, the eddy was considerably

**Fig. 9** (a) and (b) L-maps, (c) and (d) SST images, (e) and (f) O-maps with the superimposed AVISO velocity field show splitting of the eddy A (yellow and black contours) in February. See caption to Fig. 8



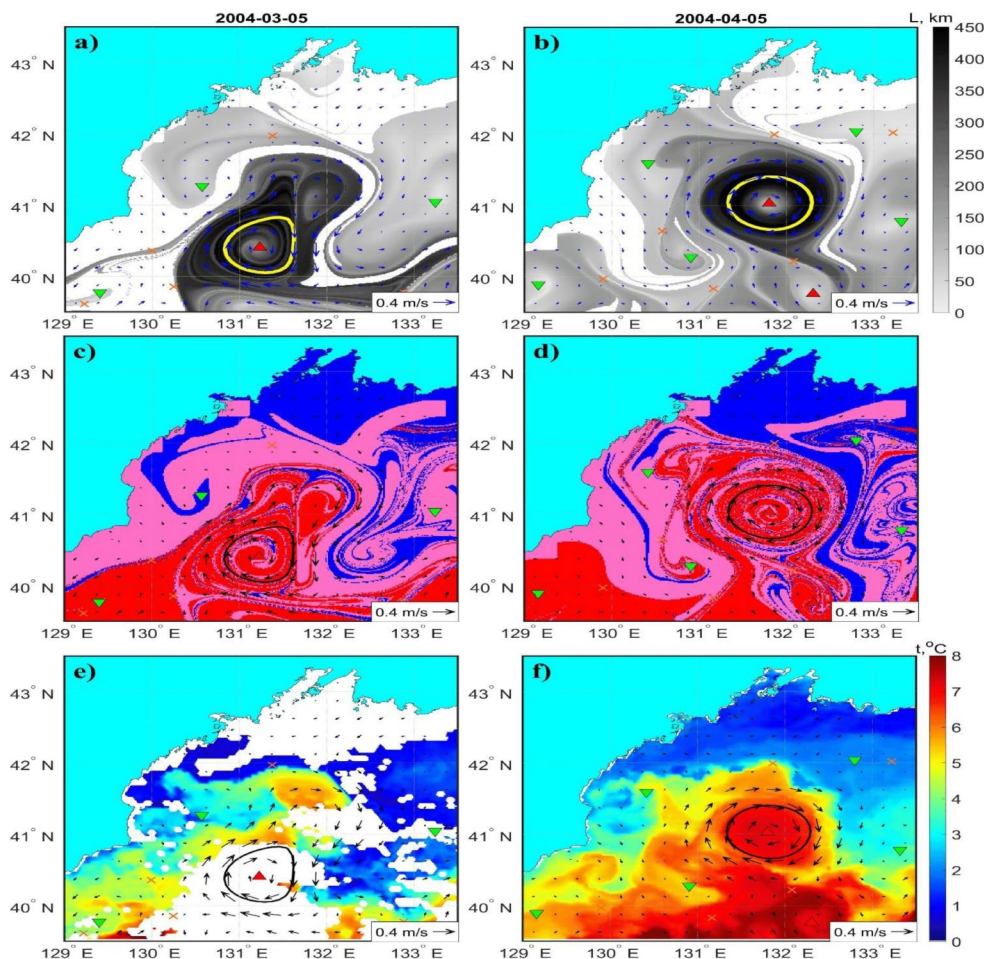
shrunk. The eddy A decayed due to interaction with the zonal eastward flow that eventually absorbed the eddy by October 10. This event was signaled by disappearance of the elliptic point within the eddy (Fig. 12c). Thus, the life of the eddy lasted nine months, from January 9 to October 10, 2004. During this long period of time, we were able to track the eddy as an entity using daily Lagrangian maps and the AMEDA eddy tracking algorithm.

To calculate the fraction of waters of different origin in the surface core, we count every day the number of subtropical, subarctic and coastal particles,  $N_{st}$ ,  $N_{sa}$  and  $N_c$

, within the characteristic vortex contour delineating the core of the eddy at the surface (see Sect. 2.2). The subtropical and subarctic particles are distinguished as those ones which crossed the zonal lines 39°N and 42.6°N from south and north, respectively, entered the study area for 365 days prior the date indicated on the plot and detected within the vortex contours. The coastal particles mark the along-shore water that has been entrained by the eddy.

In Fig. 13a we plot the fractions of subtropical, subarctic and coastal waters in the eddy core over its lifetime that were calculated by dividing  $N_{st}$ ,  $N_{sa}$  and  $N_c$  by the current

**Fig. 10** (a) and (b) L-maps, (c) and (d) O-maps, (e) and (f) SST images with the superimposed AVISO velocity field show enlargement of the eddy A (yellow and black contours) in March due to entrainment of waters of different origin. See caption to Fig. 8



value of the area under the vortex contour. During the lifetime of the eddy, the surface core has been filled mainly with the subtropical water originated in the southern flank of the Subpolar Front. It is consistent with the O-maps in Figs. 8, 9, 10 and 11 which show the subtropical water by red color. The episodes with cardinal changes of the fractions of water of different origin in Fig. 13 can be compared with the Lagrangian maps on the same dates. An entrainment of the ‘rose’ coastal water begun from February 9. That is reflected in Fig. 13a as a rapid increase of portion of coastal water in the eddy core by February 13 due to the decline in the content of subtropical water. Starting from this date, a small amount of subarctic water appears in the core for the first time. The coastal water made up a significant portion of the surface core water until the middle of August (see Fig. 13a and the T-map in Fig. 12b, where this water is shown in grey).

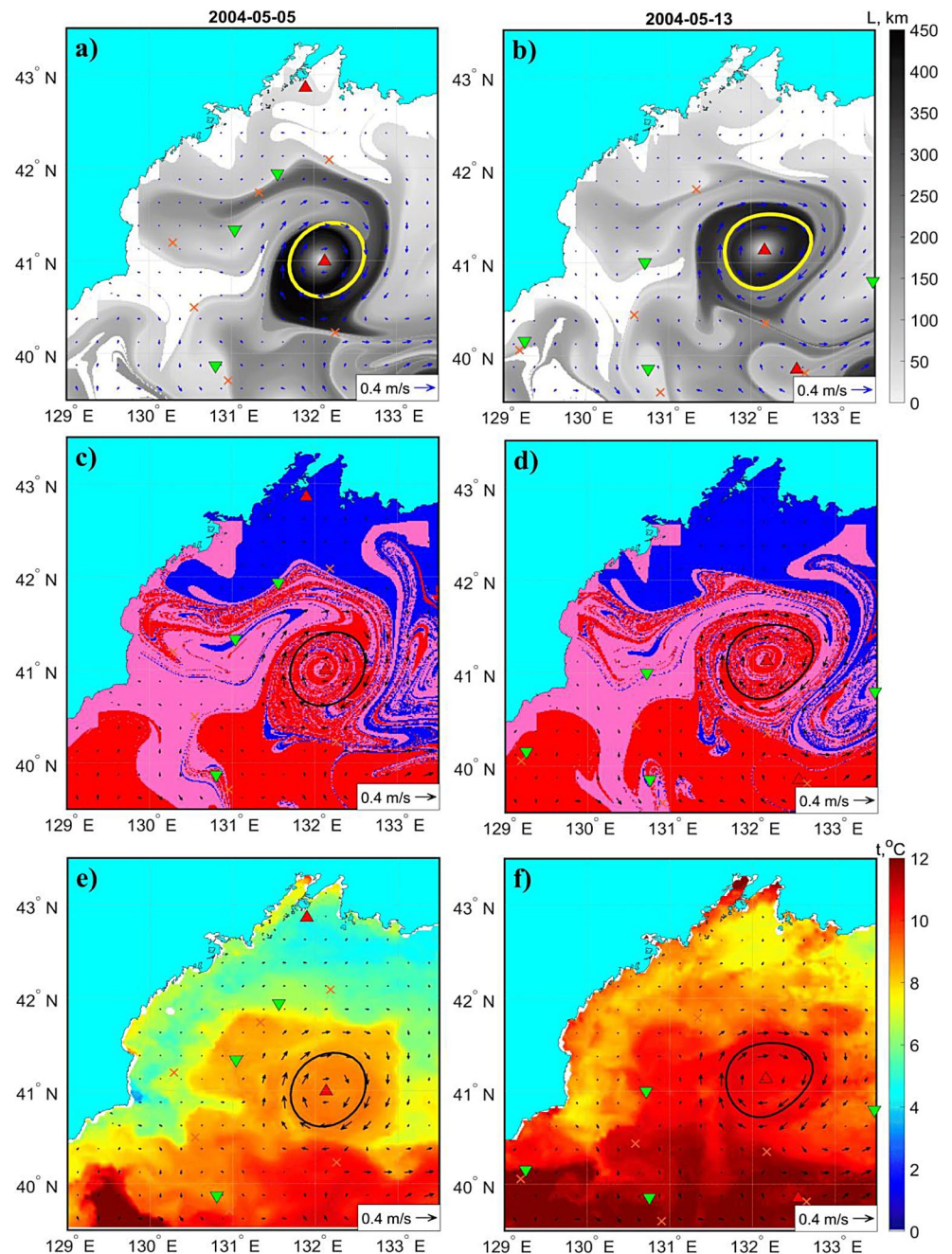
The next intrusion of coastal water to the location of the studied eddy occurred in May, when the eddy was sampled. It was not very significant event with the fraction of the coastal water within interior of the eddy increased by 10% only (see Fig. 13). The O-maps in Fig. 11c and d and the ‘age’ map in Fig. 12a show that the rose particles begun

to move from the coast and wrapped onto the eddy from the beginning of May. The eddy retained a little fraction of this water within its interior (see Fig. 11d). Inspection of the surface velocity field in May, based on the data of the GLO-RYS12V1 reanalysis, has shown a meandering of the zonal flow along the Subpolar Front that transported water from the coast to the location of the studied eddy.

The final decrease of the content of the subtropical water within the eddy occurred in the end of its life (see Fig. 13a and the T-map in Fig. 12c). As to subarctic water, its amount in the surface core was practically the same from February 13 and by the eventual decay.

The area within the characteristic vortex contour rapidly increased after the formation of the eddy and reached approximately 100 km in size by the middle of January. The maximum size of ~120 km was recorded by the middle of February after an entrainment of a large amount of subtropical and coastal waters. Just after that, the eddy destabilized and split into two parts. The erosion of the eddy begun in the beginning of July when it decreased in size from 100 km to 50 km for a month. The eventual decay started in the beginning of October and finished on October 10 (see Fig. 12d).

**Fig. 11** (a) and (b) L-maps, (c) and (d) O-maps, (e) and (f) SST images with the superimposed AVISO velocity field show entrainment of subtropical and coastal waters by the eddy (yellow and black contours) in May. See caption to Fig. 8



The strength of an eddy can be characterized by the values of the Okubo-Weiss parameter that is the sum of the squares of normal and shear strain minus the relative vorticity at a given point. Figure 14 shows the evolution of the averaged value of this parameter in the surface core that is negative over the lifetime of the eddy A. The contribution of the relative vorticity started to increase just after formation of the eddy (see also Fig. 8). The contribution of deformation has gradually increased from the beginning by the middle of February when the eddy strongly deformed due to the entrainment of the ‘rose’ coastal water (see also Fig. 13a). Then the eddy A lost its stability, starting to split in the

middle of February (see Fig. 9) with a sharp decrease of its area (see Fig. 13b). The absolute value of the Okubo-Weiss parameter reached fast the maximum value by the beginning of March (see also Fig. 9). The next sharp increase of the relative vorticity occurred in the second half of March when the eddy has gradually grown in size (see also Fig. 10).

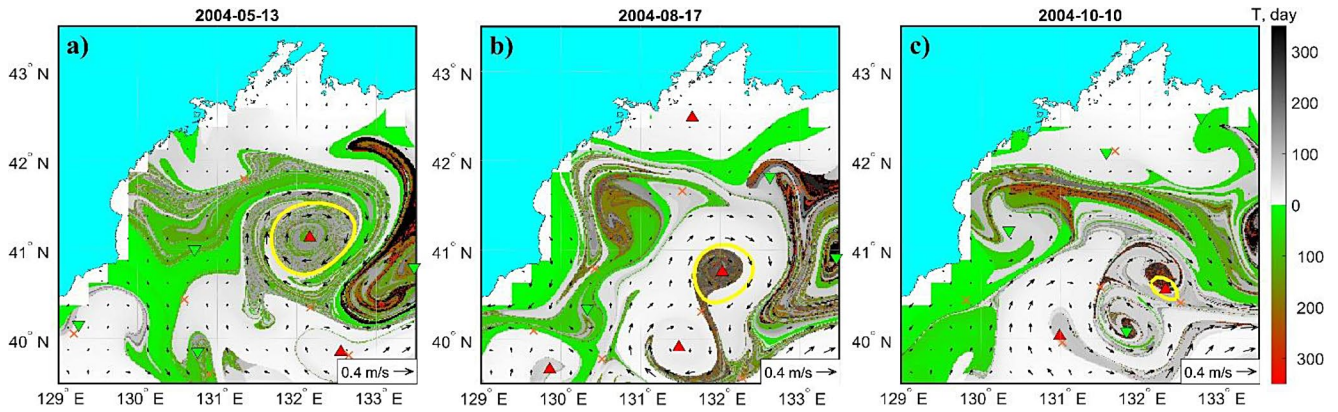


**Fig. 12** The ‘water-age’ T-maps show how ‘old’ is the water inside the studied eddy shown by the yellow contour. Three events in its biography are demonstrated: (a) sampling on May 13, when the eddy had a maximum lateral size, (b) interaction of the weakened eddy with an anticyclone of the Subpolar Front on August 17 and (c) eventual decay

on October 10. The legend of colors: shades of the grey color represent the ‘age’ of subtropical water in days, whereas variations from green to rose colors represent the ‘age’ of coastal water. The rectangular segments along the coast are the AVISO grid cells where the velocity field is poorly defined

**Fig. 13** (a) The fractions of subtropical (red), subarctic (blue) and coastal (rose) waters inside the surface core during the lifetime of the eddy. (b) The area of the surface core of the eddy during its lifetime. The vertical dashed lines show the main events during the lifetime of the eddy: F means its formation in the beginning of January, E – entrainment of coastal water and splitting in the middle of February, S – sampling in May, D – decay in October

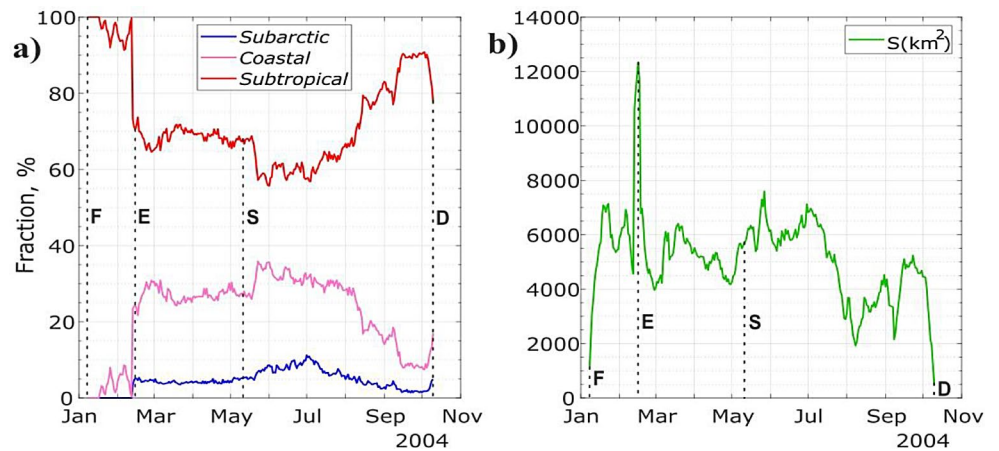
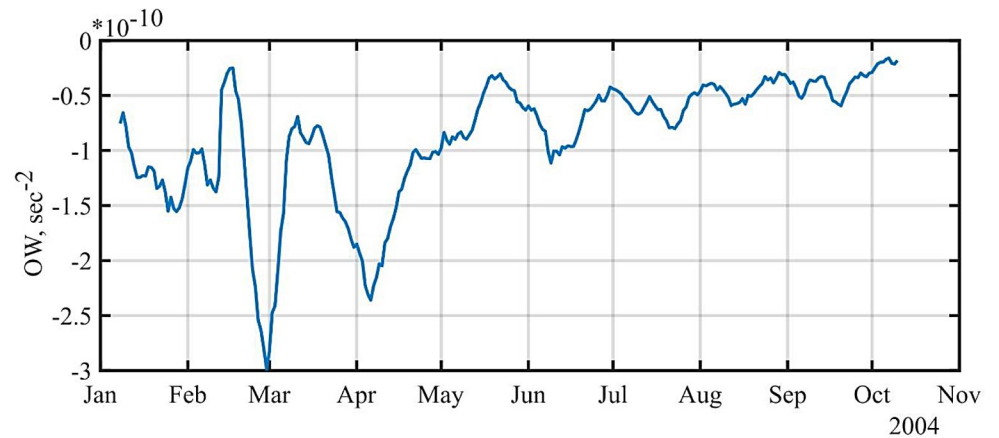


**Fig. 14** The evolution of the Okubo-Weiss parameter during the lifetime of the eddy (in  $sec^{-2} \times 10^{-10}$ )



### 5 Discussion

We used the Lagrangian approach to study the evolution of an ACE in the northwestern JS. On the one hand, this eddy was formed in the region near the Subpolar Front where mesoscale eddies regularly appear and circulated.

On the other hand, it was an exceptional long-lived feature observed with Lagrangian data over 9 months. The eddy was a strong dynamic feature with the diameter reaching 120 km and extended vertically down to the bottom that was sampled in details with CTD observations.

We have demonstrated a multilayer structure of this eddy based on ship observations. The eddy had a core of warm and low salinity water between 250 and 400 m which is typical for the eddies observed in the northwestern JS earlier (Lobanov et al. 2007). However, we found other anomalies in its structure which had not been observed before including a core of warm and relatively high salinity water between 30 and 230 m, that was slightly warmer and saline as compared to the surroundings, and surface water above the seasonal pycnocline. These anomalies in a vertical composition of different water masses in the eddy could be explained by the peculiarities of its evolution.

Using the Lagrangian approach, we have studied the eddy evolution over 9 months since January through October 2004. Based on daily-computed L- maps and maps of water origin and water ‘age’ we found a few events of entrainment of surrounding water by the eddy, splitting and merger with neighbor eddies. These events were confirmed by satellite infrared images.

Our analysis demonstrated that an entrainment of subtropical water from the south into the eddy dominated during the whole period of its evolution. It was especially strong in the beginning and in the end of the eddy life cycle, in January and in October. Just after formation and isolation of the eddy from the stream of subtropical water, an entrainment of the coastal water has increased. Subarctic water from the north was also observed to be entrained into the eddy, however its volume was around ten times lower as compared to that of subtropical water. Large entrainment of surrounding water into the eddy in February caused its rapid enlargement and splitting into two parts later in this month. Entrainment of surface water from the south, from the area of the Subpolar Front just prior the ship observation was responsible for formation of surface warm water in the upper 0–30 m observed in the middle of May (WI in Fig. 6a).

It is however difficult to explain the origin of higher salinity water in the upper core (HS1 in Fig. 6b) and the origin of lower salinity core (LS in Fig. 6b). The first water mass could be formed during the process of formation of the eddy in January (Fig. 8c and e). The second one could be the result of entrainment and subduction of low salinity intermediate water from the north. It is difficult to judge on the subsurface entrainment and subduction processes using the Lagrangian approach based on the satellite altimetry.

Meanwhile, the entrainment of warm water during the merger events or by streamers may be a mechanism that supplies potential energy and maintains long lifetime of ACEs. We have observed the studied eddy by Lagrangian data over 9 months. This exceeds the estimates provided by Lee et al. (2019) where the authors estimated the average lifetime of ACEs to be 74 days in the western Japan Basin and 95 days in the whole JS. The estimates, however, depend on the

method of eddy identification that was used in a particular study. Based on satellite infrared images, we traced ACEs in the northwestern JS during a few months and in some cases for more than 1 year (Lobanov et al., 1998; Lobanov et al. 2007). The recent study, based on altimetry data, showed that the average lifetime of 361 ACEs, observed in JS during 1993–2020 was 202 days with the maximum value of 1496 days (Zhabin et al. 2023). It is known that the lifetime of mesoscale eddies in other parts of the World Ocean may exceed 2–3 years (e.g., Olson 1991; Prants et al. 2015; Gnevyshev et al. 2021). The mesoscale eddies in JS are less energetic compared with the rings of Gulf Stream and Agulhas eddies and thus should have shorter lifetime. However, a large number of eddies circulating in JS, frequent interaction between the eddies and with frontal features, and entrainment of low density water may provide additional energy to sustain long lifetime of some ACEs. On the other hand, interaction between the eddies, splitting and merger events may limit their lifetime.

Because our simulation results are based eventually on the AVISO velocity field which is imperfect by many reasons, we need to discuss the adequacy of the Lagrangian results in representing reality. First of all, we compared these results, when possible, with observation data and infrared images. Moreover, we have not computed trajectories of the particles that reached the coastal AVISO grid cells of the size of  $1/4^\circ \times 1/4^\circ$  where the altimetric velocity field is unreliable. These trajectories stopped when reaching the coastal grid cells. The second evidence of the reliability of the results obtained is more sophisticated. The altimetric velocity field in active dynamical areas is, in principle, chaotic (turbulent). Regarding the simulation of particle’s trajectories, it is impossible to obtain ‘true’ trajectories in a chaotic and imperfect velocity field. Even if it would be absolutely perfect, it is impossible to do this because of the exponential sensitivity of output results on small variations in initial conditions. However, in strongly chaotic systems each numerically computed trajectory stays uniformly close to some ‘true’ trajectory with a slightly altered initial position (see, e.g., Ott 2002). A computed trajectory is ‘shadowed’ by a ‘true’ one. If a dense set of particles is launched, then we can be sure that there is always a computed trajectory that is everywhere close to the corresponding ‘true’ one. Thus, computed pathways for a large number of particles approximate real pathways of the transported water.

Lagrangian particle tracking with the similar linear and bilinear interpolations, we used for surface geostrophic currents in time and space, has been performed by Pak et al. (2018) in the southern JS based on satellite-observed absolute dynamic topography. The comparisons between the tracks of real drifters and simulated trajectories deployed on similar dates (see Fig. 2 by Pak et al. 2018) suggested that

the particle trajectories have shown relatively weak influences of the AVISO error terms. More than 20 drifter tracks have shown a good agreement with the trajectories during 1999–2004.

Lagrangian maps in Figs. 8, 9, 10, 11, 12 and 13 demonstrate some fine features around eddies, such as narrow rings and filaments, with a submesoscale width. In spite of the nominal resolution of the altimetric product of  $1/4^\circ \times 1/4^\circ$ , these features are structurally stable if they arise due to mesoscale advection, but not locally due to, for example, submesoscale frontogenesis. In the first case, they are robust to errors in the velocity field. This is valid if the velocity between the AVISO grid nodes changes approximately in phase with the velocity at nearby nodes. Then, those submesoscale rings and filaments arise as subtle features of the mesoscale advection in a quasi two-dimensional velocity field.

As to simulating the processes within the eddy, it should be stressed that a large-scale velocity field is smooth and regular there. It allowed us to identify the eddy center with a good accuracy exceeding the nominal resolution of the geostrophic field. Comparing the coordinates of the eddy center in the sampling sections in Fig. 3 ( $41^\circ 09'N$  and  $131^\circ 15'E$ ) with the calculation of the coordinates of the elliptic point on the days of sampling in Fig. 9b ( $41^\circ 08'N$  and  $131^\circ 11'E$ ), we may conclude that they coincide with the good accuracy.

## 6 Conclusion

The Lagrangian tools have been applied to study in detail an anticyclonic eddy in the northwestern Japan Sea with a strong dynamic feature that was sampled during the cruise in May 2004. The altimetry-based eddy tracking showed that it lived for nine months with the size reaching 100–120 km. The eddy's characteristics and vertical structure have been studied based on CTD observational data, Lagrangian analysis and satellite data. The eddy had a multilayer structure with a few cores of relatively uniform water with different temperature and salinity characteristics located in its upper layer and intermediate depth (30–400 m). Origin of these cores were associated with the interaction of the eddy with the surrounding waters and neighbor eddies and fronts that caused entrainment of water inside the eddy.

Inspecting daily-computed L- maps and maps of water origin and 'age', we documented formation of this eddy, splitting, merger, entrainment and detrainment of water, erosion and eventual decay. All these events have been confirmed by infrared satellite images. A new Lagrangian method has been applied to calculate day by day the fractions of coastal waters and waters of subtropical and subarctic origin within the eddy core. It has been found that

during the evolution the surface core has been filled mainly with the subtropical water originated in the southern flank of the Subpolar Front. The episodes with cardinal changes of ratio of different water masses have been recorded and verified with the help of Lagrangian maps. The entrainment of subtropical water by the eddy may be a mechanism that provides potential energy supporting its long lifetime.

**Acknowledgements** The work of MB, SP and AU was supported by the Russian Science Foundation (project no. 23-17-00068). Numerical codes were elaborated within the State Task No. 124022100072-5. SL and VL were supported by the State Task No. 124022100079-4. The authors acknowledge research team and the crew of R/V Akademik M.A. Lavrentyev (cruise No.33) and especially Dr. Anatoly Salyuk for CTD observations as well as our colleagues at Seoul National University and especially Profs. K. Kim and K.R. Kim and Dr. D.J. Kang who contributed a partial fund for this cruise through the Korean CREAMS program.

**Author contributions** M.B. computed and analyzed Lagrangian maps, S.L. provided and processed satellite images, V.L. carried out the eddy sampling and wrote the text, S.P. designed the research, wrote the paper and provided the funding, A.U. developed the codes to track eddies. All authors have read and agreed to the published version of the manuscript.

**Data availability** The data obtained, generated and analysed are available from the corresponding author upon reasonable request.

## Declarations

**Conflict of interest** The authors declare no conflict of interest.

## References

- Chang KI, Teague WJ, Lyu SJ, Perkins HT, Lee DK, Watts DR, Kim YB, Mitchell DA, Lee CM, Kim K (2004) Circulation and currents in the southwestern East/Japan Sea: overview and review. *Prog Oceanogr* 61:105–156. <https://doi.org/10.1016/j.pocean.2004.06.005>
- Chang KI, Zhang CI, Park C et al (2016) *Oceanography of the East Sea (Japan Sea)*. Springer
- Chelton DB, Schlax M, Samelson RM (2011) Global observations of nonlinear mesoscale eddies. *Prog Oceanogr* 91:167–216. <https://doi.org/10.1016/j.pocean.2011.01.002>
- Ginzburg AI, Kostyanoi AG, Ostrovskiy AG (1998) Surface circulation of the Japan Sea (satellite information and drifting buoys data). *Issledovanie Zemli Iz Kosmosa*. (Russian J Remote Sens) 66–83
- Gnevyshev VG, Malysheva AA, Belonenko TV, Koldunov AV (2021) On Agulhas eddies and Rossby waves travelling by forcing effects. *Russ J Earth Sci* 21:ES5004. <https://doi.org/10.2205/2021ES000773>
- Gordon AL, Giulivi CF, Lee CM, Bower A, Furey HH, Talley LD (2002) Japan/East Sea intra-thermocline eddies. *J Phys Oceanogr* 32(6):1960–1974
- Hogan PJ, Hurlburt HE (2006) Why do intrathermocline eddies form in the Japan/East Sea? A modeling perspective. *Oceanogr* 19(3):134–143

- Isoda Y (1994) Warm eddy movements in the eastern Japan Sea. *J Oceanogr* 50(1):1–16
- Isoda Y, Nishihara M (1992) Behavior of warm eddies in the Japan Sea. *Umi Sora* 67(1):231–243
- Isoda Y, Naganobu M, Watanabe H, Nukata K (1992) Horizontal and vertical structures of a warm eddy above the Yamato rise. *Umi no Kenkyu* 1:141–151 (in Japanese)
- Ivankova VN, SamoiloVA AE (1979) New fish species for the USSR waters and an invasion of heat-loving fauna in the north-western part of the Japan Sea. *Voprosy Ihtiologii* 19:449–550
- Kim YG, Kim K (1999) Intermediate waters in the East/Japan Sea. *J Oceanogr* 55(2):123–132
- Kim T, Jo HJ, Moon JH (2021) Occurrence and evolution of mesoscale thermodynamic phenomena in the northern part of the East Sea (Japan Sea) derived from satellite altimeter. *Remote Sens* 13(6):1071. <https://doi.org/10.3390/rs13061071>
- Le Vu B, Stegner A, Arsouze T (2018) Angular momentum Eddy Detection and Tracking Algorithm (AMEDA) and its application to Coastal Eddy formation. *J Atmos Ocean Tech* 35(4):739–762. <https://doi.org/10.1175/JTECH-D-17-0010.1>
- Lee DK, Niiler PP (2005) The energetic surface circulation patterns of the Japan/East Sea. *Deep Sea Res Part II* 52:1547–1563. <https://doi.org/10.1016/j.dsr2.2003.08.008>
- Lee DK, Niiler P (2010) Eddies in the southwestern East/Japan Sea. *Deep Sea Res Part I* 57:1233–1242. <https://doi.org/10.1016/j.dsr.2010.06.002>
- Lee GM, Thomas LN, Yoshikawa Y (2006) Intermediate water formation at the Japan/East Sea Subpolar front. *Oceanogr* 19(3):110–121
- Lee K, Nam S, Kim YG (2019) J Korean Soc Oceanogr 24:267–281 (in Korean). <https://doi.org/10.7850/jkso.2019.24.2.267>. Statistical Characteristics of East Sea Mesoscale Eddies Detected, Tracked, and Grouped Using Satellite Altimeter Data from 1993 to 2017
- Lobanov VB, Danchenkov MA, Nikitin AA (1998) On the role of mesoscale eddies in the Japan Sea water mass transport and modification. *J Oceanogr* 11(2):46
- Lobanov VB, Ponomarev VI, Salyuk AN, Tishchenko PY, Talley LD (2007) Structure and dynamics of synoptic scale eddies in the northern Japan Sea. *Far Eastern Seas of Russia*, Ed. V.A. Akulichchev. V. 1. Oceanographic Research. Nauka: Moscow. 450–473 (in Russian)
- Mitchell DA, Teague WJ, Wimbush M, Watts DR, Sutyrin GG (2005) The Dok Cold Eddy. *J Phys Oceanogr* 35:273–288. <https://doi.org/10.1175/jpo-2684.1>
- Morimoto A, Yanagi T, Kaneko A (2000) Eddy field in the Japan Sea derived from satellite altimetric data. *J Oceanogr* 56:449–462
- Nikitin AA, Lobanov VB, Danchenkov MA (2002) Possible ways of warm subtropical water transport into the area of Far Eastern Marine preserve. *Izv TINRO* 131:41–53 (in Russian)
- Nikitin AA, Yurasov GI, Vanin NS (2012) Satellite observations of synoptic eddies and the geostrophic circulation of the sea of Japan waters. *Izv Atmos Ocean Phy* 48(9):980–992
- Olson DB (1991) Rings in the Ocean. *Annu Rev Earth Planet Sci* 19:283–311. <https://doi.org/10.1146/annurev.ea.19.050191.001435>
- Ott E (2002) *Chaos in Dynamical systems*. Cambridge University Press, Cambridge
- Ou HW, Gordon A (2002) Subduction along a midocean front and the generation of intrathermocline eddies: a theoretical study. *J Phys Oceanogr* 32(6):1975–1986
- Pak G, Kim YH, Park YG (2018) Lagrangian Approach for a new separation index of the East Korea warm current. *Ocean Sci J* 54:29–38. <https://doi.org/10.1007/s12601-018-0059-2>
- Park AK, Chung JY (1999) Spatial and temporal scale variations of sea surface temperature in the East Sea using NOAA/AVHRR data. *J Oceanogr* 271–288
- Park KA, Chung JY, Kim K (2004) Sea surface temperature fronts in the East (Japan) Sea and temporal variations. *Geophys Res Lett* 31:L07304. <https://doi.org/10.1029/2004gl019424>
- Pegliasco C, Delepouille A, Mason E, Morrow R, Faugère Y, Dibarboure G (2022) META3.1exp: a new global mesoscale eddy trajectory atlas derived from altimetry. *Earth Syst Sci Data* 14:1087–1107. <https://doi.org/10.5194/essd-14-1087-2022>
- Ponomarev VI, Fayman PA, Prants SV, Budyansky MV, Uleysky M (2018) Simulation of mesoscale circulation in the Tatar Strait of the Japan Sea. *Ocean Model* 126:43–55. <https://doi.org/10.1016/j.ocemod.2018.04.006>
- Prants SV, Uleysky MYu, Budyansky MV (2017b) Lagrangian Oceanography: large-scale transport and mixing in the Ocean. *Physics of Earth and Space environments*. Springer, Berlin, Germany
- Prants SV, Ponomarev VI, Budyansky MV, Uleysky My, Fayman PA (2015) Lagrangian analysis of the vertical structure of eddies simulated in the Japan Basin of the Japan/East Sea. *Ocean Model* 86:128–140. <https://doi.org/10.1016/j.ocemod.2014.12.010>
- Prants SV, Budyansky MV, Uleysky M (2017a) Statistical analysis of Lagrangian transport of subtropical waters in the Japan Sea based on AVISO altimetry data. *Nonlin Processes Geophys* 24:89–99. <https://doi.org/10.5194/npg-24-89-2017>
- Prants SV, Fayman PA, Budyansky MV, Uleysky MY (2022) Simulation of Winter Deep Slope Convection in Peter the Great Bay (Japan Sea). *Fluids* 7:134. <https://doi.org/10.3390/fluids7040134>
- Preller RH, Hogan PJ (1998) In: Robinson AR, Brink KH (eds) *Oceanography of the Sea of Okhotsk and the Japan/East seas*. The Sea. V. 11. Eds. John Wiley and Sons Inc, pp 429–481
- Schlitzer R (2023) *Ocean Data View*, <https://odv.awi.de>
- Shin CW (2009) Characteristics of a warm Eddy observed in the Ulleung Basin in July 2005. *Ocean Polar Res* 31:283–296. <https://doi.org/10.4217/opr.2009.31.4.283>
- Shin HR, Shin CW, Kim C et al (2005) Movement and structural variations of warm eddy WE92 for three years in the western East/Japan Sea. *Deep-Sea Res II* 52(11–13):1742–1762
- Sugimoto T, Tameishi H (1992) Warm core rings, streamers and their role in the fishing ground formation around Japan. *Deep Sea Res Part I Oceanogr Res Pap* 183–201. [https://doi.org/10.1016/S0198-0149\(11\)80011-7](https://doi.org/10.1016/S0198-0149(11)80011-7)
- Takematsu M, Ostrovski AG, Nagano Z (1999) Observations of eddies in the Japan basin interior. *J Oceanogr* 55:237–246. <https://doi.org/10.1023/a:1007846114165>
- Talley LD, Min DH, Lobanov VB, Luchin V, Ponomarev V, Salyuk A, Shcherbina A, Tishchenko P, Zhabin I (2006) Japan/East Sea Water Masses and their relation to the Sea's circulation. *J Oceanogr* 19(3):32–49. <https://doi.org/10.5670/oceanog.2006.42>
- Trusenkova O, Kaplunenko D (2022) Intra-annual sea level fluctuations and variability of mesoscale processes in the Northern Japan/East Sea from satellite altimetry data. *Front Mar Sci* 866328–866460. <https://doi.org/10.3389/fmars.2022.866328>
- Uda M (1934) The results of simultaneous oceanographic investigations in the Japan Sea and its adjacent waters in May and June 1932. *J Imperial Fisheries Experimental Stn* 5:57–190
- Wagawa T, Kawaguchi Y, Igeta Y, Honda N, Okunishi T, Yabe I (2020) Observations of oceanic fronts and water-mass properties in the central Japan Sea: repeated surveys from an underwater glider. *J Mar Syst* 201:103242. <https://doi.org/10.1016/j.jmarsys.2019.103242>
- Watanabe T, Hirai M, Yamada H (2001) High-salinity intermediate water of the Japan Sea in the eastern Japan Basin. *J Geophys Res* 106(C6):11437–11450. <https://doi.org/10.1029/2000JC000398>
- Yabe I, Kawaguchi Y, Wagawa T, Fujio S (2021) Anatomical study of Tsushima warm current: determination of principal pathways and its variation. *Prog Oceanogr* 194:102590. <https://doi.org/10.1016/j.pocean.2021.102590>

- Yarichin VG (1980) The contemporary knowledge on the circulation in the Japan Sea (Sostoyanie Izuchennosti Tsirkulyatsii Vod Yaponskogo morya). *Trudy DVNIGMI* 80:46–61 (in Russian)
- Yoon JH, Kim YJ (2009) Review on the seasonal variation of the surface circulation in the Japan/East Sea. *J Mar Syst* 78:226–236. <https://doi.org/10.1016/j.jmarsys.2009.03.003>
- Yoshikawa Y, Lee CM, Thomas LN (2012) The Subpolar Front of the Japan/East Sea. Part III: competing roles of Frontal Dynamics and Atmospheric forcing in driving Ageostrophic Vertical circulation and subduction. *J Phys Oceanogr* 42(6):991–101. <https://doi.org/10.1175/JPO-D-11-0154.1>
- Yurasov GI, Yarichin VG (1991) Currents of the Japan Sea (Techeniya Yaponskogo morya). *FEC AS USSR, Vladivostok*. (in Russian)
- Zhabin IA, Dmitrieva EV, Taranova SN, Lobanov VB Circulation and Mesoscale Eddies in the Sea of Japan from Satellite Altimetry Data., *Izvestiya (2023) Atmospheric and Oceanic Physics*, 2023, Vol. 59, No. 10, pp. 1409–1426. <https://doi.org/10.1134/S0001433823120253>
- Zhao N, Manda A, Han Z (2014) Frontogenesis and frontolysis of the subpolar front in the surface mixed layer of the Japan Sea. *J Geophys Res* 119:1498–1509. <https://doi.org/10.1002/2013JC009419>

**Publisher's Note** Springer Nature remains neutral with regard to jurisdictional claims in published maps and institutional affiliations.

Springer Nature or its licensor (e.g. a society or other partner) holds exclusive rights to this article under a publishing agreement with the author(s) or other rightsholder(s); author self-archiving of the accepted manuscript version of this article is solely governed by the terms of such publishing agreement and applicable law.